

Polarization-induced 2D hole gases in pseudomorphic undoped GaN/AlN heterostructures on single-crystal AlN substrates

Cite as: Appl. Phys. Lett. **119**, 162104 (2021); doi: [10.1063/5.0066072](https://doi.org/10.1063/5.0066072)

Submitted: 7 August 2021 · Accepted: 6 October 2021 ·

Published Online: 19 October 2021










View Online



Export Citation



CrossMark

Zexuan Zhang,^{1,a)}  Jimy Encomendero,^{1,b)}  Reet Chaudhuri,¹  Yongjin Cho,¹  Vladimir Protasenko,¹ Kazuki Nomoto,¹ Kevin Lee,¹  Masato Toita,² Huili Grace Xing,^{1,3,4}  and Debdeep Jena^{1,3,4} 

AFFILIATIONS

¹School of Electrical and Computer Engineering, Cornell University, Ithaca, New York 14853, USA

²Advanced Devices Technology Center, Asahi Kasei Corporation, Hibiya Mitsui Tower, 1-1-2 Yurakucho, Chiyoda-ku, Tokyo 100-8440, Japan

³Department of Materials Science and Engineering, Cornell University, Ithaca, New York 14853, USA

⁴Kavli Institute at Cornell for Nanoscale Science, Ithaca, New York 14853, USA

Note: This paper is part of the APL Special Collection on Wide- and Ultrawide-Bandgap Electronic Semiconductor Devices.

^{a)}Author to whom correspondence should be addressed: zz523@cornell.edu

^{b)}Electronic mail: jj64@cornell.edu

ABSTRACT

A high-conductivity two-dimensional (2D) hole gas is the enabler of wide-bandgap p-channel transistors. Compared to commonly used AlN template substrates with high dislocation densities, the recently available single-crystal AlN substrates are promising to boost the speed and power handling capability of p-channel transistors based on GaN/AlN 2D hole gases (2DHGs) thanks to the much lower dislocation densities and the absence of thermal boundary resistance. Using plasma-assisted molecular beam epitaxy, we report the observation of polarization-induced high-density 2DHGs in undoped pseudomorphic GaN/AlN heterostructures on the single-crystal AlN substrates with high structural quality and atomic steps on the surface. The high-density 2DHG persists down to cryogenic temperatures with a record high mobility exceeding $280 \text{ cm}^2/\text{V s}$ and a density of $2.2 \times 10^{13}/\text{cm}^2$ at 10 K. These results shed light on aspects of improving 2D hole mobilities and indicate significant potential of GaN/AlN 2DHG grown on bulk AlN substrates for future high performance wide-bandgap p-channel transistors.

Published under an exclusive license by AIP Publishing. <https://doi.org/10.1063/5.0066072>

A strong need exists for a wide-bandgap p-type transistor counterpart of the n-channel GaN high electron mobility transistors (HEMTs) for power electronics and high-voltage digital RF CMOS circuits.^{1–6} The p-channel transistor counterpart has proven to be difficult,¹ since the wide bandgap of GaN leads to high hole effective masses and deep valence bands, which are difficult to dope and difficult to contact with typical metal workfunctions.^{2,7–9} Among the various structures proposed as a platform for p-channel III-Nitride electronics,^{3,4,10–12} the polarization-induced 2D hole gases (2DHG) at GaN/AlN hetero-interface has received recent attention. The low sheet resistance (because of the very high density 2DHG) and extreme voltage-handling capability (as a result of the high thermal conductivity and high breakdown electric field of GaN and AlN) in this structure lead to the recent demonstration of the first nitride p-channel

transistors that break the GHz speed barrier (with $f_T/f_{max} \sim 20 \text{ GHz}$), and currents exceeding 400 mA/mm .¹

The substrates used for epitaxial growth of GaN/AlN 2DHG heterostructures in previous studies have been AlN templates on sapphire.³ The large lattice mismatch between AlN and the substrate (typically sapphire or SiC) results in a high density ($\sim 10^9 - 10^{10} \text{ cm}^{-2}$) of dislocations. These dislocations affect the mobility of 2D holes by acting as scattering centers. In addition, they also contribute to leakage currents in AlN based transistors, degrade the breakdown voltages, and limit high power operation.^{13,14} One method to mitigate this problem is to use lattice-matched single crystal AlN substrates. Recently, bulk AlN single-crystals grown by physical vapor transport (PVT) with dislocation densities $< 10^4 \text{ cm}^{-2}$ (6 orders lower than that of AlN templates) have become available.^{15,16} Homoepitaxy on single

crystal AlN substrates can remove the undesired thermal boundary resistance (TBR) at the AlN/SiC (sapphire) interface.¹⁷ TBR has been found to be one of the limiting factors for efficient heat dissipation of GaN based high power devices.^{18–21} A large TBR increases the temperature rise in the device channel and degrades performance and reliability. Therefore, a 2DHG at GaN/AlN interface on a structurally pure single-crystal AlN substrate is of scientific interest to better understand the role of disorder on the transport properties of 2D holes and also of technological interest for exploring the speed and power handling limits of nitride p-channel transistors.

In this work, we report epitaxial growth of undoped pseudomorphic GaN/AlN heterostructures on single-crystal AlN substrates by plasma-assisted molecular beam epitaxy (MBE) with smooth surface morphology. The presence of polarization-induced 2DHGs in these structures was confirmed by temperature dependent Hall-effect measurements. The low temperature mobility of the 2D holes in this study grown on single-crystal AlN substrates is higher than all earlier reports for similar structures grown on AlN/sapphire templates³ and reaches as high as $> 280 \text{ cm}^2/\text{V s}$ at 10 K. We believe that this is the highest reported hole mobility in GaN to date.

The MBE growth of the epitaxial structures in this study was performed in a Veeco GENxplor MBE system. High purity elemental Al and Ga effusion cells supplied the metal fluxes, and ultra-high purity nitrogen gas was supplied through a rf plasma source. KSA Instruments reflection high-energy electron diffraction (RHEED) apparatus with a Staib electron gun operating at 14.5 kV and 1.45 Å was used to *in situ* monitor the film growth.

The bulk substrates used in this study are Al-polar AlN substrates with dislocation densities $< 10^4/\text{cm}^2$ from Crystal IS.¹⁵ Following the same *ex situ* cleaning procedure as outlined in our previous work,²² diced AlN substrates of area of $1 \times 1 \text{ cm}^2$ were mounted on faceplates and loaded into the MBE system and out-gassed at 200 °C for 8 h.

Prior to the growth of epi-layers, *in situ* chemical cleaning of the substrate was first performed in the MBE growth chamber in a background pressure of $\sim 10^{-9}$ Torr without the nitrogen gas flow. The substrate was heated up to a thermocouple temperature of 950 °C and then exposed to an aluminum metal flux of 10 nm/min for 30 s. The high temperature was held long enough for the deposited Al to desorb. Such process of adsorption and desorption of Al was repeated for 20 cycles. This Al-assisted cleaning has been found to be effective in deoxidizing AlN bulk substrate surfaces for achieving true homoepitaxial growth by MBE.^{16,22}

After the *in situ* Al-assisted cleaning, a 700 nm AlN buffer layer was grown at a thermocouple temperature of 910 °C with the Al beam equivalent pressure (BEP) of 5.8×10^{-7} Torr and nitrogen plasma operating at 200 W with the N_2 gas flow rate of 1.95 sccm. Excess Al droplets were *in situ* desorbed at an elevated thermocouple temperature of 940 °C (monitored by RHEED intensity change) before cooling down the substrate to a thermocouple temperature of 700 °C. Following the deposition of a 100 nm undoped $\text{Al}_{0.95}\text{Ga}_{0.05}\text{N}$ layer and the *in situ* desorption of excess Ga droplets, the 500 nm AlN buffer layer and the 13.5 nm GaN layer were deposited under metal-rich conditions without growth interruption. The substrate was then immediately cooled down to room temperature. The excess Ga droplets were *ex situ* removed by HCl. The reason for metal-rich condition during GaN growth is to have excess Ga accumulating on the surface. The

excess Ga acts as a surfactant to help to achieve a smooth surface and suppress initial elastic relaxation.^{23,24}

The purpose of the high Al content AlGa_N layer is to prevent unwanted silicon donor dopants “floating” on the growth front of the AlN under the Al-rich growth condition from reaching and compensating the GaN/AlN heterojunction where the 2DHG is desired.^{25,26} A schematic layer structure is shown in Fig. 1(a). A simulation using a self-consistent 1D Schrödinger–Poisson solver suggests the presence of a high density polarization-induced 2DHG at the GaN/AlN interface, as shown in Fig. 1(b). Figure 1(c) shows the RHEED pattern viewed along GaN (11 $\bar{2}$ 0) azimuth by the end of the growth at 700 °C. The streaky RHEED pattern indicates the smooth surface and high crystallinity of the epitaxial structure in this study.

The structural quality of the epitaxial structure is characterized by x-ray diffraction (XRD) using a Panalytical XPert Pro setup at 45 kV and 40 mA with Cu K α 1 radiation (1.5406 Å). Figure 2(a) shows the measured symmetric $2\theta/\omega$ XRD scan of the sample, along with the simulated diffraction pattern based on the layer structure shown in Fig. 1(a). The simulation has been offset for clarity. A good agreement between the measured and simulated result is observed. The clearly visible interference fringes suggest abrupt hetero-interfaces. The reciprocal space map (RSM) around the asymmetric (105) diffractions of GaN and AlN shown in Fig. 2(b) suggests that the GaN layer is fully strained to the underlying AlN layer.

The surface morphology of the material stack was measured using atomic force microscopy (AFM) in an Asylum Research Cypher ES setup. Smooth surface morphology with a root mean square (rms) roughness of 0.6 nm in a $10 \times 10 \mu\text{m}^2$ AFM scan can be seen in Fig. 3(a). No spiral hillocks or surface pits were observed. This surface morphology is distinct from earlier reports grown on AlN/sapphire templates, where a high density of spiral hillocks was observed.³ Since the spiral hillocks are known to be signatures of dislocations for AlN homoepitaxy, similar to metal-rich GaN epitaxy,^{16,27} the absence of spiral hillocks in this study indicates a significantly reduced density of dislocations. Furthermore, the $2 \times 2 \mu\text{m}^2$ AFM scan in Fig. 3(b) shows the presence of smooth and parallel atomic steps. The inset shows a line scan height profile along the black line in Fig. 3(b). The height of each step is very close to the one monolayer thickness of c-plane GaN. This further suggests the step-flow growth mode in this study and corroborates the high structural quality of the epi-layers.

Temperature dependent Hall-effect measurement was conducted in van der Pauw geometry on as-grown GaN/AlN heterostructure samples with indium dots as the contacts under 1 Tesla magnetic field to examine properties of the hole gas in this structure. A positive sign of the Hall coefficient was observed at all measured temperatures, confirming the presence of p-type conductivity. Figure 4(a) shows the evolution of the hole density extracted from Hall-effect measurements as a function of temperature. The hole density shows a moderate dependence on temperature, decreasing from $p_s = 4.7 \times 10^{13}/\text{cm}^2$ at 290 K to $p_s = 2.2 \times 10^{13}/\text{cm}^2$ at 10 K. Similar temperature dependence of hole density was also observed in a previous report grown on AlN/sapphire templates.³ The measured hole density at 290 K is consistent with the calculated value of $p_s \sim 4.7 \times 10^{13}/\text{cm}^2$ [shown by the gray dashed line in Fig. 4(a)] using self-consistent Schrödinger–Poisson simulation, if the surface Fermi level is ~ 1.9 eV above the valence band of GaN at room temperature, as has been recently measured using contactless electroreflectance (CER) technique.²⁸ This moderate

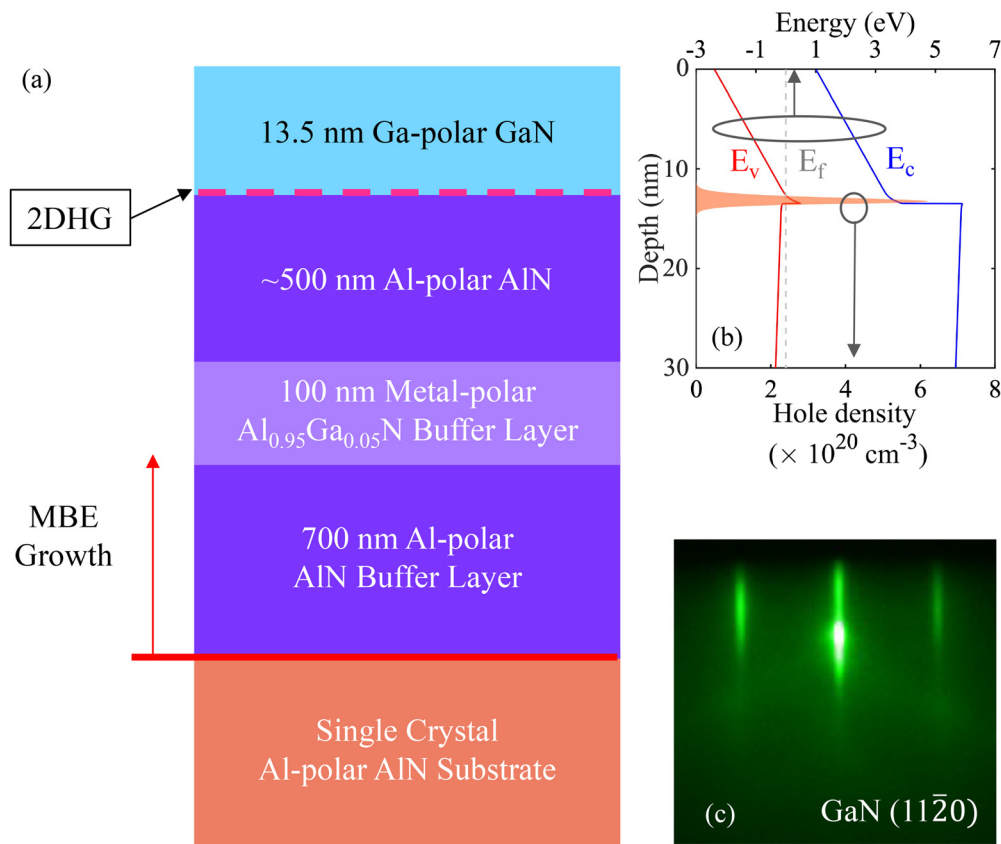


FIG. 1. (a) Schematic of the epitaxial structure in this study. (b) Calculated band diagram and hole gas density at GaN/AlN interface by self-consistent Schrödinger–Poisson simulation. (c) RHEED pattern viewed along GaN (11 $\bar{2}$ 0) azimuth by the end of the growth.

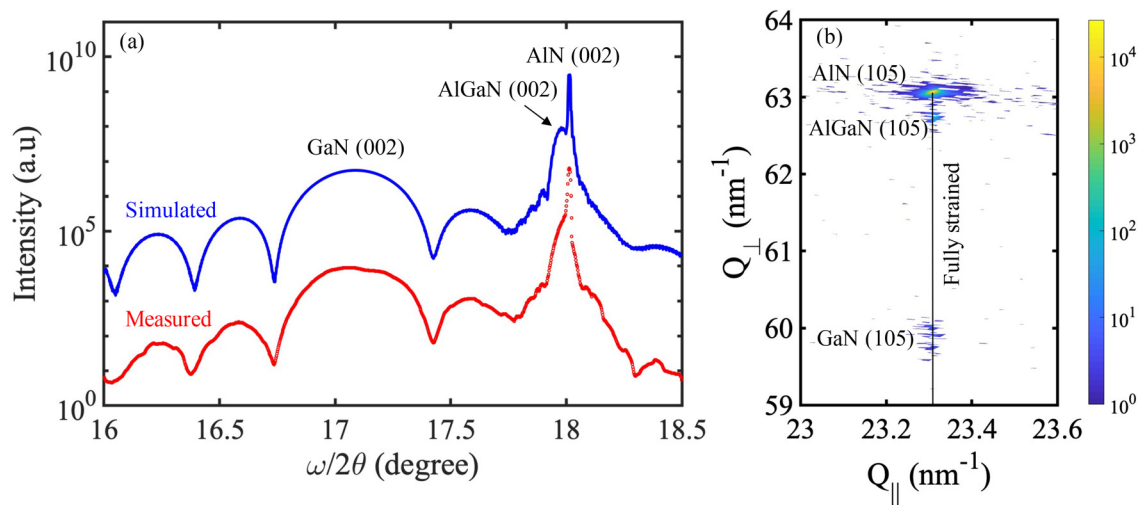


FIG. 2. (a) Measured (red) and simulated (blue) symmetric $2\theta/\omega$ x-ray diffraction (XRD) scan across the (002) diffraction for the sample structure in this study. The simulated result has been offset for clarity. (b) Reciprocal space map scan of the asymmetric (105) diffractions of GaN and AlN shows that the GaN layer is fully strained to the AlN layer.

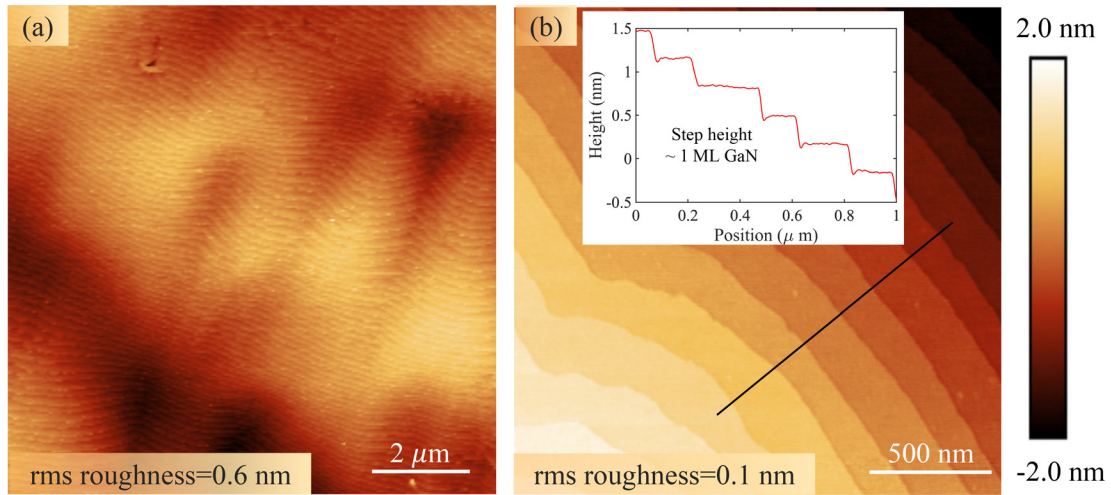


FIG. 3. (a) $10 \times 10 \mu\text{m}^2$ AFM image of the as-grown surface with root mean square (rms) roughness ~ 0.6 nm. (b) $2 \times 2 \mu\text{m}^2$ AFM image with rms roughness ~ 0.1 nm shows the presence of parallel and smooth atomic steps. Inset: line scan height profile along the black line shows each step height ~ 1 monolayer of c-plane GaN.

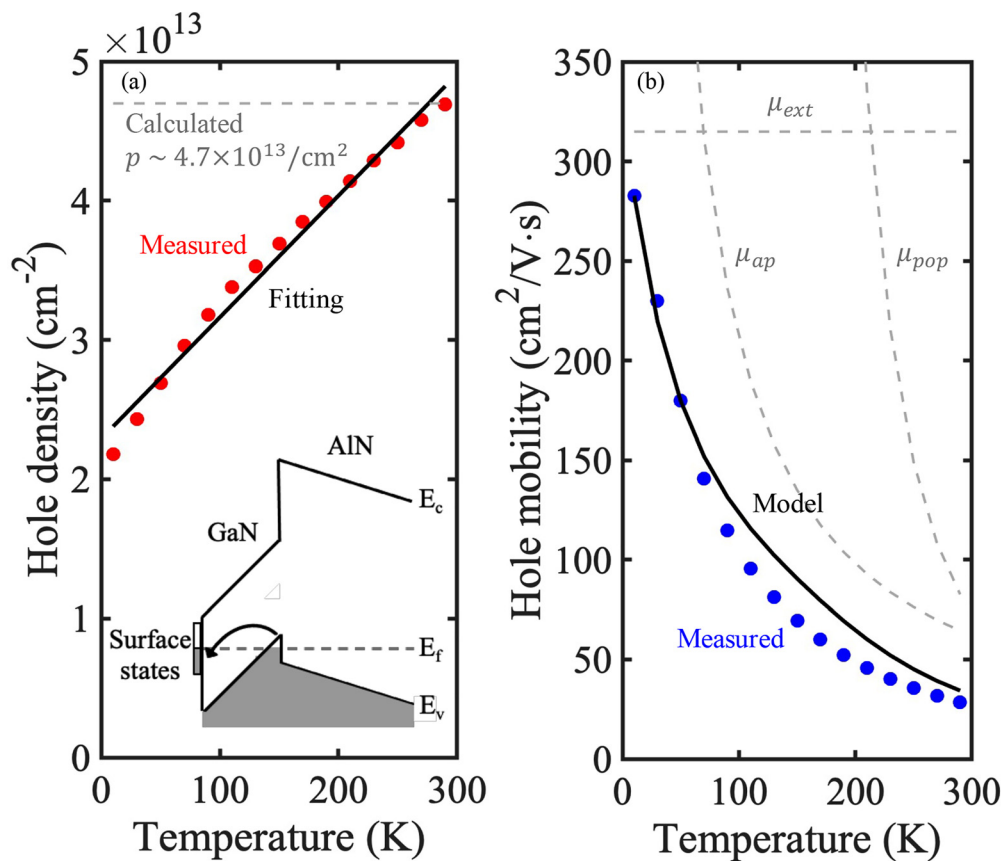


FIG. 4. (a) Measured hole density from Hall-effect measurements as a function of temperature (red circles) and linear fitting (black line). Gray dashed line indicates the calculated hole density of $p_s \sim 4.7 \times 10^{13}/\text{cm}^2$ at room temperature. Inset: schematic of the possible source of 2DHG. (b) Measured (blue circles) and calculated (black curve) hole mobility vs temperature. Gray dashed lines show the individual contributions from acoustic phonons (μ_{ap}), optical phonons (μ_{pop}), and other extrinsic mechanisms (μ_{ext}), respectively.

temperature dependence of the hole density is in sharp contrast to the exponential dependence observed in Mg-doped control samples³ and confirms the polarization-induced nature of the 2DHG in this study. A linear fitting [black line in Fig. 4(a)] of the temperature dependent hole gas density $p_s(T) = p_s(0\text{ K}) + \alpha T$ gives $p_s(0\text{ K}) = 2.3 \times 10^{13}/\text{cm}^2$ and $\alpha = 8.7 \times 10^{10} \text{ cm}^{-2} \text{ K}^{-1}$. The origin behind the temperature dependence of hole density is still under investigation at this point. One possible scenario could be the temperature dependent charge transfer between *localized* surface states and the 2DHG. Assume that there exist localized acceptor-like surface states (which do not contribute to transport) in thermal equilibrium with the 2DHG in the valence band (which contribute to transport). With the decreasing temperature, some of the holes will transfer from the GaN/AlN interface to these localized surface states in order to maintain thermal equilibrium as well as charge neutrality. This is equivalent to electrons from the surface states filling the hole states (empty states in the valence band). Future exploration on how the temperature dependence of 2DHG density varies under different surface treatment conditions (such as surface passivation) is under way and will be of high value to evaluate this hypothesis.

We mention the potential *source* of the 2DHG in this GaN/AlN heterostructure. Because holes represent empty states in the valence band, the *source* of the 2DHG is in essence the *sink* of valence band electrons. We hypothesize that surface states act as the sink of valence band electrons in the GaN/AlN heterostructure with a GaN surface exposed to air. Specifically, electrons from the valence band go to unoccupied localized states on the surface. The inset of Fig. 4(a) shows a schematic of such a process. If instead of a bare surface, a metal gate is deposited, then the large polarization field transfers electrons from the valence band to the empty states of the metal above its intrinsic Fermi level. If, on the other hand, defects exist in the GaN layer or the AlN layer below Fermi level inside the bandgap, the valence band electron could be transferred there. We think that this is unlikely because of the high-speed ($\sim 20 - 40$ GHz) response of p-type field effect transistors (pFETs) would not be possible if this was the case. Furthermore, assuming that such defect states spread over ~ 10 nm from the interface, a 2DHG density of $\sim 4 \times 10^{13}/\text{cm}^2$ would require $\sim 4 \times 10^{19}/\text{cm}^3$ deep traps, which is also unlikely.

Figure 4(b) shows the temperature dependence of hole mobility from Hall-effect measurements. The 10 K hole mobility exceeds $280 \text{ cm}^2/\text{V s}$. We believe that this is the highest hole mobility reported in GaN to date. The mobility of the 2D holes in GaN/AlN heterostructure has been theoretically studied in a previous report using a *numerical* approach.⁷ The low temperature mobility of holes is limited by extrinsic scattering mechanisms, including interface roughness, dislocations, and impurities, whereas phonon scattering (both acoustic and optical phonons) dominate at higher temperatures.⁷ Here, we consider a simplified model by assuming that all the 2D holes occupy a *single* heavy hole (HH) band and scatter with phonon modes in GaN. Though in reality, holes occupying the light hole (LH) band also contribute to the transport,⁷ this single band approximation allows an *analytical* description of phonon scattering and agrees reasonably well with the experimental data (as shown later).

Under an effective mass approximation, the acoustic-phonon limited hole mobility μ_{ap} for 2D holes at temperature T is given by²⁹

$$\mu_{ap} \approx \frac{16e\rho v_s^2 \hbar^3}{3k_B T D_{ac}^2 m_h^2 b(p_s)}, \quad (1)$$

where e is the electron charge, k_B is the Boltzmann constant, \hbar is the reduced Planck constant, $D_{ac} = 6.2 \text{ eV}$ is the acoustic phonon deformation potential,²⁵ $\rho = 6.15 \times 10^3 \text{ kg/m}^3$ is the GaN mass density, $V_s = 7963 \text{ m/s}$ is the sound velocity in GaN, $m_h = 2m_0$ is the heavy hole effective mass in GaN⁷ (with m_0 the free electron rest mass), p_s is the 2DHG density, and $b(p_s) = [(33m_h e^2 p_s)/(8\hbar^2 \epsilon_0 \kappa_0)]^{1/3}$ is the variational Fang–Howard wavefunction parameter that quantifies the spatial spread of the 2DHG (κ_0 is the low-frequency dielectric constant of GaN).

The optical-phonon limited hole mobility μ_{pop} for 2D holes at temperature T can be expressed as³⁰

$$\mu_{pop} \approx \frac{\kappa^* \epsilon_0 k_0 \hbar^2}{2\pi e \omega_0 m_h^2 N G(k_0)} \left(1 + \frac{1 - e^{-y}}{y} \right), \quad (2)$$

where $\kappa^* = 1/(1/\kappa_\infty - 1/\kappa_0)$ (with $\kappa_\infty = 5.4$ the high-frequency dielectric constant and $\kappa_0 = 8.9$ the low-frequency dielectric constant of GaN), ϵ_0 is the vacuum permittivity, $\hbar\omega_0 = 92 \text{ meV}$ is the optical phonon energy in GaN, $k_0 = \sqrt{2m_h\omega_0/\hbar}$ is the hole wave vector corresponding to the optical phonon energy, N is the Bose–Einstein distribution function $N(T) = 1/[\exp(\hbar\omega_0/k_B T) - 1]$, $y = \pi\hbar^2 p_s/m_h k_B T$, and $G(k_0)$ is the form factor given by $G(k_0) = b(8b^2 + 9k_0 b + 3k_0^2)/8(k_0 + b)^3$.

Note that because of the heavily degenerate 2DHG concentration, the Hall factor is unity, and the calculated field effect mobility can be compared directly with the Hall-effect mobility. Mobility limited by extrinsic scattering mechanisms (μ_{extr}), such as interface roughness, dislocations, and impurities, is considered to be *independent* of temperature⁷ and is used as a “tuning parameter.” The black curve in Fig. 4(b) shows the calculated hole mobility as a function of temperature by combining all the aforementioned scattering mechanisms using Matthiessen’s rule. An acceptable agreement between the calculated values and experimental data is achieved with $\mu_{extr} = 320 \text{ cm}^2/\text{V s}$. This value is higher than $\mu_{extr} \sim 200 \text{ cm}^2/\text{V s}$ for GaN/AlN 2DHG grown on AlN/sapphire templates in earlier reports.^{3,7} Since μ_{extr} includes scattering by dislocations, the increase in μ_{extr} from AlN/sapphire template substrates to AlN bulk substrates is expected due to a reduced density of dislocations on AlN bulk substrates. Chemical analysis, such as secondary ion mass spectrometry (SIMS), will be an important future direction to compare the impurity levels at GaN/AlN interface when grown on AlN bulk substrates and AlN/sapphire template substrates.

To better understand the impact of the substrate on the transport properties of 2DHGs at GaN/AlN interface, the hole density and hole mobility of multiple samples (including the ones grown on AlN bulk substrates in this work and those grown on AlN/sapphire templates from Ref. 3) at 300, 77, and 10 K are compared in Fig. 5. 2DHGs are observed in multiple samples grown on AlN bulk substrates with *reproducible* transport properties. As shown by the gray dashed lines in Fig. 4(b), the hole mobility at high temperature is limited mainly by phonon scattering. As a result, various samples show similar hole mobilities at 300 K, independent of the substrate. In contrast, the low temperature hole mobility is limited by extrinsic mechanisms, such as interface roughness, dislocation, and impurity scattering. This explains why the low temperature (77 and 10 K) mobilities of the 2DHGs grown on AlN bulk substrates with reduced density of dislocations consistently exceed those grown on AlN/sapphire templates as seen in Fig. 5. The sheet resistances of all samples show metallic behavior and

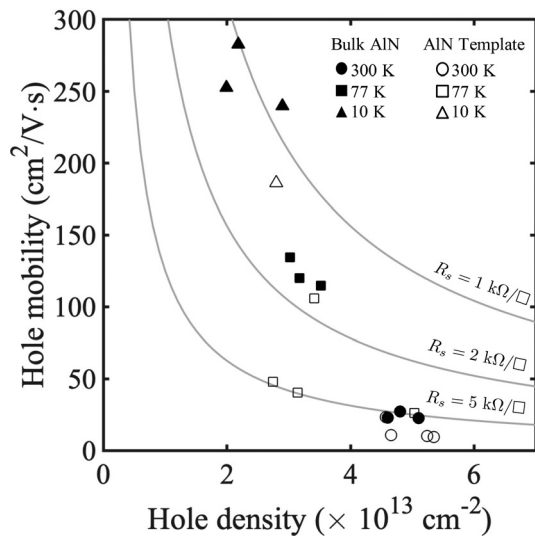


FIG. 5. Comparison of hole density and hole mobility at 300 (circle), 77 (square), and 10 K (triangle) between undoped, polarization-induced 2D hole gases grown on bulk AlN substrates in this work (filled symbols) and those grown on AlN/sapphire templates from Ref. 3 (empty symbols).

decrease monotonically with the decreasing temperature. Thanks to the higher hole mobility, the samples grown on AlN bulk substrates in this study show repeatably lower sheet resistances than the ones grown on AlN/sapphire templates across the whole temperature range from 10 to 300 K. The lowest sheet resistances achieved in this work are $4.8 \text{ k}\Omega/\square$ at 300 K and $0.9 \text{ k}\Omega/\square$ at 10 K. Low sheet resistance is desired for high speed, high performance p-channel devices,^{1,2,6} and this again highlights an advantage of the bulk AlN platform.

In conclusion, epitaxial growth of undoped pseudomorphic GaN/AlN heterostructures on single crystal AlN substrates were achieved by plasma-assisted MBE. Temperature-dependent Hall-effect measurements confirm the existence of polarization-induced 2DHGs at the GaN/AlN heterojunction. The measured hole density shows a moderate dependence on temperature, consistent with its polarization-induced origin. The sharp hetero-interface, smooth surface morphology, and the low dislocation density ($<10^4/\text{cm}^2$) of AlN bulk substrates enable the observation of record high hole mobility in GaN ($> 280 \text{ cm}^2/\text{V}\cdot\text{s}$ at 10 K). Moreover, the thermal boundary resistance between AlN and other substrates (which limits the performance and reliability of devices) is naturally absent on the bulk AlN platform. These results, together with the recent demonstration of high-power X-band (with output power of $15.2 \text{ W}/\text{mm}$) and W-band (with output power of $2.2 \text{ W}/\text{mm}$ at 94 GHz) n-channel HEMTs on the same AlN platform,^{31,32} offer significant hope to take this wide-bandgap CMOS platform into unexplored application domains in the RF and power electronics arenas.⁶ For example, logic blocks enabled by this GaN/AlN 2DHG could be monolithically integrated with the existing high-speed wide-bandgap power switches as control circuitry. Such integration can help to eliminate the parasitics, reduce the system complexity, and further boost the overall performance of GaN based power integrated circuits.^{33,34}

The authors at Cornell University acknowledge financial support from Asahi Kasei, the Cornell Center for Materials

Research (CCMR)—a NSF MRSEC program (No. DMR-1719875); ULTRA, an Energy Frontier Research Center funded by the U.S. Department of Energy (DOE), Office of Science, Basic Energy Sciences (BES), under Award No. DE-SC0021230; and AFOSR Grant No. FA9550-20-1-0148. This work uses the CESI Shared Facilities partly sponsored by NSF No. MRI DMR-1631282 and Kavli Institute at Cornell (KIC).

AUTHOR DECLARATIONS

Conflict of Interest

The authors have no conflicts of interest to declare.

Author Contributions

Z. Z. and J.E. contributed equally to this work.

DATA AVAILABILITY

The data that support the findings of this study are available from the corresponding author upon reasonable request.

REFERENCES

- K. Nomoto, R. Chaudhuri, S. Bader, L. Li, A. Hickman, S. Huang, H. Lee, T. Maeda, H. Then, M. Radosavljevic *et al.*, in *IEEE International Electron Devices Meeting (IEDM)* (IEEE, 2020), pp. 8–3.
- S. J. Bader, R. Chaudhuri, K. Nomoto, A. Hickman, Z. Chen, H. W. Then, D. A. Muller, H. G. Xing, and D. Jena, *IEEE Electron Device Lett.* **39**, 1848 (2018).
- R. Chaudhuri, S. J. Bader, Z. Chen, D. A. Muller, H. G. Xing, and D. Jena, *Science* **365**, 1454 (2019).
- R. Chu, Y. Cao, M. Chen, R. Li, and D. Zehnder, *IEEE Electron Device Lett.* **37**, 269 (2016).
- N. Chowdhury, Q. Xie, M. Yuan, K. Cheng, H. W. Then, and T. Palacios, *IEEE Electron Device Lett.* **41**, 820 (2020).
- S. J. Bader, H. Lee, R. Chaudhuri, S. Huang, A. Hickman, A. Molnar, H. G. Xing, D. Jena, H. W. Then, N. Chowdhury *et al.*, *IEEE Trans. Electron Devices* **67**, 4010 (2020).
- S. J. Bader, R. Chaudhuri, M. F. Schubert, H. W. Then, H. G. Xing, and D. Jena, *Appl. Phys. Lett.* **114**, 253501 (2019).
- J. O. Song, J.-S. Ha, and T.-Y. Seong, *IEEE Trans. Electron Devices* **57**, 42 (2010).
- S. Wahid, N. Chowdhury, M. K. Alam, and T. Palacios, *Appl. Phys. Lett.* **116**, 213506 (2020).
- M. Shatalov, G. Simin, J. Zhang, V. Adivarahan, A. Koudymov, R. Pachipulusu, and M. A. Khan, *IEEE Electron Device Lett.* **23**, 452 (2002).
- T. Zimmermann, M. Neuburger, M. Kunze, I. Daumiller, A. Denisenko, A. Dadgar, A. Krost, and E. Kohn, *IEEE Electron Device Lett.* **25**, 450 (2004).
- G. Li, R. Wang, B. Song, J. Verma, Y. Cao, S. Ganguly, A. Verma, J. Guo, H. G. Xing, and D. Jena, *IEEE Electron Device Lett.* **34**, 852 (2013).
- T. Kikkawa, K. Makiyama, T. Ohki, M. Kanamura, K. Imanishi, N. Hara, and K. Joshin, *Phys. Status Solidi A* **206**, 1135 (2009).
- Y. Yamaoka, A. Ubukata, Y. Yano, T. Tabuchi, K. Matsumoto, and T. Egawa, *Semicond. Sci. Technol.* **34**, 035015 (2019).
- Z. Zhang, M. Kushimoto, T. Sakai, N. Sugiyama, L. J. Schowalter, C. Sasaoka, and H. Amano, *Appl. Phys. Express* **12**, 124003 (2019).
- Y. Cho, C. S. Chang, K. Lee, M. Gong, K. Nomoto, M. Toita, L. J. Schowalter, D. A. Muller, D. Jena, and H. G. Xing, *Appl. Phys. Lett.* **116**, 172106 (2020).
- Z. Su, J. P. Freedman, J. H. Leach, E. A. Preble, R. F. Davis, and J. A. Malen, *J. Appl. Phys.* **113**, 213502 (2013).
- A. Sarua, H. Ji, K. Hilton, D. Wallis, M. J. Uren, T. Martin, and M. Kuball, *IEEE Trans. Electron Devices* **54**, 3152 (2007).
- A. Manoi, J. W. Pomeroy, N. Killat, and M. Kuball, *IEEE Electron Device Lett.* **31**, 1395 (2010).

- ²⁰K. Park and C. Bayram, *Appl. Phys. Lett.* **109**, 151904 (2016).
- ²¹K. Filippov and A. Balandin, *Mater. Res. Soc. Internet J. Nitride Semicond. Res.* **8**, 4 (2003).
- ²²K. Lee, Y. Cho, L. J. Schowalter, M. Toita, H. G. Xing, and D. Jena, *Appl. Phys. Lett.* **116**, 262102 (2020).
- ²³G. Mula, C. Adelman, S. Moehl, J. Oullier, and B. Daudin, *Phys. Rev. B* **64**, 195406 (2001).
- ²⁴C. Adelman, J. Brault, G. Mula, B. Daudin, L. Lymperakis, and J. Neugebauer, *Phys. Rev. B* **67**, 165419 (2003).
- ²⁵R. Chaudhuri, Z. Chen, D. A. Muller, H. G. Xing, and D. Jena, *J. Appl. Phys.* **130**, 025703 (2021).
- ²⁶K. Lee, R. Page, V. Protasenko, L. J. Schowalter, M. Toita, H. G. Xing, and D. Jena, *Appl. Phys. Lett.* **118**, 092101 (2021).
- ²⁷B. Heying, E. Tarsa, C. Elsass, P. Fini, S. DenBaars, and J. Speck, *J. Appl. Phys.* **85**, 6470 (1999).
- ²⁸Ł. Janicki, R. Chaudhuri, S. J. Bader, H. G. Xing, D. Jena, and R. Kudrawiec, *Phys. Status Solidi RRL* **15**, 2000573 (2021).
- ²⁹J. H. Davies, *The Physics of Low-Dimensional Semiconductors: An Introduction* (Cambridge university Press, 1998).
- ³⁰B. Gelmont, M. Shur, and M. Strosio, *J. Appl. Phys.* **77**, 657 (1995).
- ³¹S. Ozaki, J. Yaita, A. Yamada, Y. Kumazaki, Y. Minoura, T. Ohki, N. Okamoto, N. Nakamura, and J. Kotani, *Appl. Phys. Express* **14**, 041004 (2021).
- ³²A. Hickman, R. Chaudhuri, N. Moser, M. Elliott, K. Nomoto, L. Li, J. C. M. Hwang, H. G. Xing, and D. Jena, in *Device Research Conference (DRC)* (IEEE, 2021).
- ³³H. Amano, Y. Baines, E. Beam, M. Borga, T. Bouchet, P. R. Chalker, M. Charles, K. J. Chen, N. Chowdhury, R. Chu *et al.*, *J. Phys. D* **51**, 163001 (2018).
- ³⁴Z. Zheng, L. Zhang, W. Song, S. Feng, H. Xu, J. Sun, S. Yang, T. Chen, J. Wei, and K. J. Chen, *Nat. Electron.* **4**, 595 (2021).